University *of Ljubljana*
Faculty *of Mathematics and Physics*

Seminar:
Casimir effect in graphene

Author: Matic Lubej
Advisor: prof. dr. Rudolf Podgornik
March 2012

Abstract:

Electromagnetic vacuum fluctuations have observable consequences, one of them being the Casimir effect. This effect produces an attractive or a repulsive force between objects[1]. These effects can today be measured with good accuracy[4]. This seminar is about the Casimir effect in graphene, a material that is massively researched in today's nanotechnology. Because it can be applied in the nanoscopic world, the fluctuation effects cannot be neglected. This paper presents the magnitudes of Casimir – van der Waals interactions for different systems of graphene layers and SiO_2 substrate arrangements. The calculations were done in the framework of Lifshitz theory, which gives the most detailed description of interactions in dielectrics[6].

Table of contents

1 Introduction

The Casimir force, or so called “the force from nothing”, is an effect which was predicted by Hendrik B. G. Casimir. But how can a force of any kind be created from “nothing”? To explain this, one has to take a step into the quantum field theory. This theory states that any electromagnetic field can be treated as an infinite set of oscillators as shown in **Fig. 1**. Because this is a quantum theory, we are dealing with quantum harmonic oscillators, which have the corresponding energy levels $E_n = \hbar\omega\left(n + \frac{1}{2}\right)$, with $\hbar$ as the reduced Planck constant. A highly oscillating field would have a large value of *n*. If we now remove the radiation and all present particles, we are left with a vacuum state with the corresponding $n = 0$. The theory states, that the zero-point expectation energy of an electromagnetic field is not zero, but $E_0 = \frac{\hbar\omega}{2}$, which is also the zero-point energy of the harmonic oscillator. Generally the energy of the vacuum is not the same as the zero-point energy, because of the fluctuations of the field, which are the cause of energy fluctuations around zero point energy.

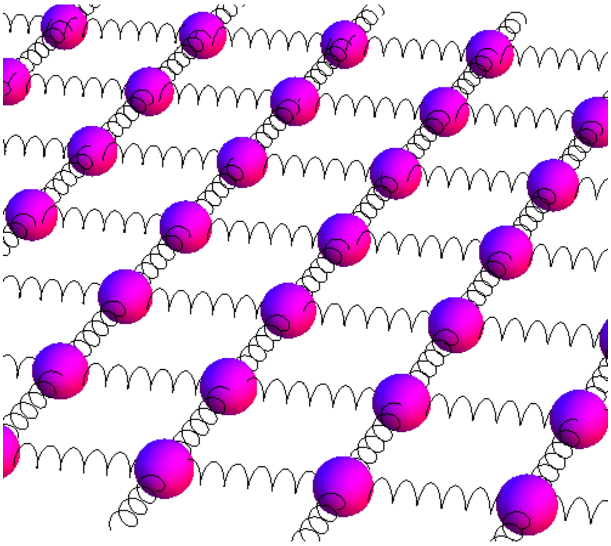

Figure 1 – A figurative schematic of a field in the form of a set of oscillators. The displacement of an oscillator is proportional to the energy of the field in that point in space.

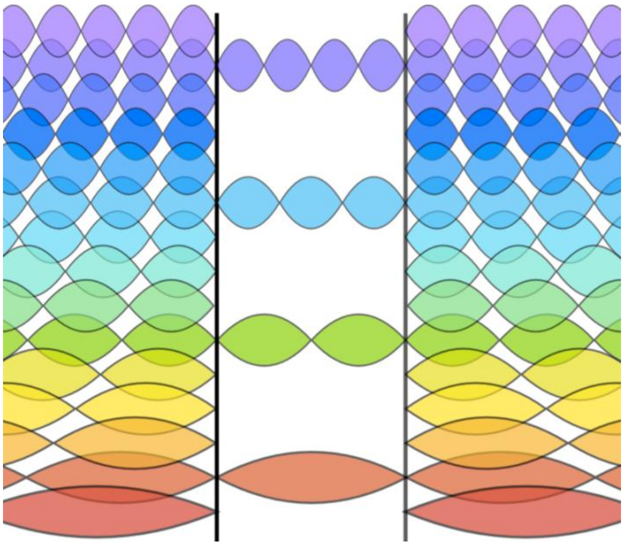

Figure 2 - A schematic presentation of oscillation modes between two metal plates, which obey boundary conditions - the magnitude of the EM field is zero on the surface of a conductor

If we put a metal cavity or two distanced plates in such fluctuations, they have to obey certain boundary conditions that depend entirely on the geometry and properties of the system as shown in **Fig. 2**. Because of these fluctuations of “nothing”, the expectation energy value between the plates is not the same as outside. This results in various effects such as the Casimir effect.

2 The Force [1]

Let us now make a closer look at this force for a special case of two ideally conducting metals, set apart at a distance *D*, that interact with all frequencies of the electromagnetic radiation. These results are valid for the temperature of absolute zero, so there is no interaction between bodies. The radiation between the plates takes a form of

$$\mathbf{E}_n(\mathbf{r},t) = \mathbf{E}_0 \cdot e^{i(\mathbf{q}\cdot\boldsymbol{\rho}-\omega_n t)} \sin(k_z z), \tag{1}$$

where the transverse wave vector is $\mathbf{q}=(k_x,k_y)$ and the transverse position vector is $\boldsymbol{\rho}=(x,y)$. Boundary conditions state that there is no EM field on the surface of a conductor, therefore equations give us

$$k_z = \frac{n\pi}{D} \qquad \text{and} \qquad \omega_n^2 = c^2k^2 = c^2\left(q^2+\frac{n^2\pi^2}{D^2}\right), \tag{2}$$

where the former is the normal component of the wave vector which satisfies the boundary conditions and the latter is a discrete spectrum of frequencies as opposed to the case of infinite empty space, where these frequencies take a form of a continuous spectrum $\omega^2 = c^2\left(q^2+k_z^2\right)$. *c* is the speed of light.

The difference of ground state energies is then defined as

$$\Delta E = \frac{1}{2}\hbar\sum_{q,n}\omega_n - \frac{1}{2}\hbar\sum_{\mathbf{k}}\omega. \tag{3}$$

If we have a large enough space, we use the identity that

$$\sum_{\mathbf{k}} f(\mathbf{k}) = \sum_{n} f(\mathbf{k}(n)) = \int d^3n\, f(\mathbf{k}(n)) = \frac{V}{(2\pi)^3}\int d^3\mathbf{k}\, f(\mathbf{k}), \tag{4}$$

where *V* is the volume of the space. **Eq. 4** takes a form of

$$\Delta E = \left[\frac{\hbar c}{2}\frac{S}{(2\pi)^2}\sum_n\int d^2\mathbf{q}\sqrt{q^2+\frac{n^2\pi^2}{D^2}} - \frac{\hbar c}{2}\frac{V}{(2\pi)^3}\int\int d^2\mathbf{q}\,dk_z\sqrt{q^2+k_z^2}\right]2, \tag{5}$$

where *S* is the surface area of the plate and the factor 2 at the end comes from the polarization effects of the waves excluding the state with n=0. If we evolve **Eq. 6** furthermore, we get

$$\Delta E = \frac{\hbar c S}{2\pi}\left(\sum_n\int_0^\infty q\,dq\sqrt{q^2+\frac{n^2\pi^2}{D^2}} - \frac{D}{\pi}\int_0^\infty\int_0^\infty q\,dq\,dk_z\sqrt{q^2+k_z^2}\right). \tag{6}$$

We should briefly stop here and note that both of these integrals are divergent, which is expected, because we have made an approximation of ideal metals that interact even with radiation with wavelengths shorter than the atomic width. For waves of this kind, real metals should be invisible roughly at $k_{\max} \approx \frac{1}{a}$, where a is the atomic width.

---

[1] This derivation of the force is from reference [5]

We renormalize the integrals by cutting the integral borders from above at the mentioned $k_{\max}$ with a cutting function defined as

$$f(k) = \begin{cases} 1\ ;\ k < k_{\max} \\ 0\ ;\ \text{otherwise} \end{cases}. \tag{7}$$

With a new integration variable $t = q^2 \frac{\pi^2}{D^2}$ and $k_z = v$, **Eq. 7** can be written as

$$\Delta E = \frac{\hbar c S \pi^2}{4D^3}\left(\sum_n \int_0^\infty dt \sqrt{t+n^2}\, f(t,v) - \int_0^\infty\int_0^\infty dt dv \sqrt{t+n^2}\, f(t,v) \right). \tag{8}$$

We now define a new function

$$F(v) = \int_0^\infty dt \sqrt{t+v^2}\, f(v,t), \tag{9}$$

so we can simplify **Eq. 9** in the form of

$$\Delta E = \frac{\hbar c S \pi^2}{4D^3}\left(\frac{1}{2}F(0) + \sum_{n=1}^\infty F(n) - \int_0^\infty F(v) dv \right). \tag{10}$$

Euler – Maclaurin summation formula states that

$$\sum_{n=1}^\infty F(n) - \int_0^\infty dv F(v) = -\frac{1}{2}F(0) - \frac{1}{12}F'(0) + \frac{1}{720}F'''(0) + ..., \tag{11}$$

where $F'(0) = 0$, $F^{(3)}(0) = -4$ and all higher derivatives are equal to zero, due to the cutting function. Finally, we are left with the famous Casimir equation

$$\Delta E = -\frac{\hbar c S \pi^2}{720 D^3}. \tag{12}$$

This energy difference is finite and does not depend on the cutting function. We can now derive the Casimir force per unit surface (Casimir pressure) as

$$\frac{F_c}{S} = \frac{d}{dD}\left(\frac{E(D)}{S}\right) = -\frac{\hbar c \pi^2}{240 D^4}. \tag{13}$$

The force is attractive and its existence implies that differences in the ground state energy of the EM field are finite and should be measurable[1].

The next logical step is calculating the magnitude of the force. At a surface area of 1cm² Casimir pressure is equal to 0.001 Pa at a distance of D = 1μm, which is equivalent to a pressure of a water droplet. But at the distance D = 10 nm, this pressure has a surprising value of 1 bar, so it should be easily observable.

In fact, various experiments for the detection of the effect have been performed:

- (1958, Netherlands) Obtained results were not contradictory, but had large experimental errors
- (1997) More accurate results of the force between a plate and a sphere[4]
- (2001, Italy) Success in measuring the force between two plates

This force is clearly a macroscopic effect predicted by the relativistic quantum field theory, otherwise known as quantum electrodynamics (QED).

3 Lifshitz theory

So far we’ve talked about a special case of ideal metal plates at absolute zero temperature. A more applicative approach would be the calculation of the Casimir effect in common materials that appear in real life. Here the dielectric permittivity is generally a function of frequency. In addition to field fluctuations, which result as Casimir effect, van der Walls interactions occur as a consequence of fluctuations in matter. To sum up, in common materials we talk about Casimir – vdW interactions, because they both occur and act together.

Evgeny Lifshizt developed a theory which is in this case very convenient to use. It is a theory of fluctuations in conductors and dielectrics[2]. We introduce the concept of free energy $\mathcal{F} = U - TS$ with U as internal energy, T as temperature and S as entropy. This is a quantity through which we can calculate the stress tensor of the interactions, and from this the corresponding force between interacting bodies. In Lifshitz theory, free energy per unit area at a finite temperature is defined as[3]

$$\frac{\mathcal{F}(l)}{S} = k_B T \sum_q \sum_{n=0}^{\infty} \ln\left[D(i\xi_n, q)\right], \tag{14}$$

where

$$D(i\xi_n, q) = 1 - \Delta_{12}(\omega)\Delta_{23}(\omega)e^{-2ql} \tag{15}$$

is the secular determinant of the system, and

$$\Delta_{ij}(\omega) = \frac{\varepsilon_i(\omega) - \varepsilon_j(\omega)}{\varepsilon_i(\omega) + \varepsilon_j(\omega)} \tag{16}$$

is the definition of dielectric discontinuity between two neighboring layers. We derive the secular determinant through the geometry of the given system while obeying boundary conditions and dielectric properties of specific layers. Eigenvalues of this determinant are the possible modes of oscillations with the corresponding dispersion relation

$$\kappa_i^2(i\xi_n) = \frac{\omega_n^2}{c^2} = q^2 + \frac{\varepsilon_i(i\xi_n)\xi_n^2}{c^2}, \tag{17}$$

where ξ_n are the Matsubara frequencies[6] $\xi_n = \dfrac{2\pi n k_B T}{\hbar}$, which are a set of possible frequencies for a bosonic system in the direction that is perpendicular to the plate. We can see that all of the frequency dependency is simplified to a sum over a set of discrete and imaginary frequencies. They also depend on temperature, which means they describe temperature effects.

4 Retardation effects

The speed of light is a finite quantity, so every signal takes a finite time to propagate from one point to another, resulting in a delay or retardation. It is important to note what these effects are and predict how they affect our calculations, so we can recognize them later, if they occur. Casimir effect arises from the fluctuations in the electromagnetic field, which propagate with the speed of light, so it is retarded by nature. On the other hand, van der Waals interactions depend on the distance between interacting bodies, so the effects are sometimes retarded or non-retarded.

It has been observed, that vdW interactions become retarded for distances larger than 10 nm [9]. As previously said, Casimir and vdW effects both contribute to the final result, so we should expect different regions where different effects take place.

Roughly three regimes occur, due to van der Waals' interaction theory. These regimes describe different dependencies of the free energy as a function of distance. They are the ***retarded***, ***non-retarded*** and the ***long distance*** region. Exact behavior of the transitions between these regions depend on the dielectric response function of doped and undoped graphene[6].The non-retarded regime are the small distances that seem insignificant when compared to the path traveled by light (ct >>b). Increasing our distances we enter the retarded regime, the previous does not apply here and effects of retardation take place. Lastly, the long distanced or the fully retarded regime occurs, which behaves as the zero frequency, classical limit.

Tab. 1 shows all scaling exponents that roughly describe the regimes in the free energy – distance dependency for the case of two semi-infinite slabs, an infinite slab and a thin sheet, and for two thin sheets. *n(b)* is the scaling exponent of our function, but more about it later. It is defined as

$$n(b) = -\frac{d \ln \mathcal{F}(b)}{d \ln b}. \tag{18}$$

Regime\Exponent	Two semi-infinite slabs	Thin sheet & semi-infinite slab	Two thin sheets
Non-retarded	n=2	n=3	n=4
Retarded	n=3	n=4	n=5
Long distance	n=2	n=3	n=4

Table 1 - A table of scaling exponents that describe the free energy dependency with respect to the distance for three regions (retarded, non-retarded, long distanced) and three different systems (slab-slab, sheet- slab, sheet-sheet).

Another regime that should be noted are the ***vanishing*** distances, which are distances comparable to atomic dimensions. The theory here loses validity, so we cannot successfully predict its outcome.

5 Graphene

Graphene is an allotrope of carbon. It is a planar sheet packed in a perfect honeycomb lattice. The structure of graphene is two dimensional and has the thickness of one carbon atom[7]. Graphene conducts electricity and its structure allows electrons to behave as massless particles that can travel at a very high speed (300 times slower than the luminal velocity)[10]. In addition, it can be doped with free charge carriers which increases its conductivity. Graphene is commonly known is commonly known in the form of which are graphene sheets stacked together with the interplanar distance of 0.335 nm[8]. These sheets have no covalent or ionic bonding between them. This is very convenient because any interlayer interactions are purely of Casimir – vdW nature and this is our main motivation for the use of this compound, in addition to the fact that it is heavily researched in today's science and has proven to be very interesting especially on various fields in nanotechnology. Graphene clearly gives us a unique opportunity to research the nature of Casimir – vdW effects.

As mentioned before, we need a known dielectric response function for graphene[2, 11]. This is obtainable through a method called random phase approximation (RPA). RPA gives the response function in the form of

$$\varepsilon(q, i\xi_n) = 1 - V(q)\chi(q, i\xi_n, \mu), \tag{19}$$

where $V(q) = \frac{2\pi e^2}{4\pi\varepsilon_0\varepsilon_m q}$ is the transverse 2D Fourier-Bessel transform of the Coulomb potential with the assumption of no interlayer Coulomb interaction in the direction perpendicular to the plates. *e* is the elementary charge, ε_0 is vacuum permittivity and ε_m is the dielectric constant for the surrounding media, which in the case of vacuum equals 1. The response functions are not the same for doped and undoped graphene.

In the case of doped graphene $\chi(q, i\xi_n, \mu)$ takes a form of

$$\begin{aligned}\chi(q, i\xi_n, \mu) = -\frac{g\mu}{2\pi(\hbar v)^2} - \frac{gq^2}{16\hbar\sqrt{\xi_n^2 + (vq)^2}} + \frac{gq^2}{8\pi\hbar\sqrt{\xi_n^2 + (vq)^2}}\Re e\left[\arcsin\left(\frac{2\mu + i\xi_n\hbar}{vq\hbar}\right) + \right. \\ \left. + \frac{2\mu + i\xi_n\hbar}{vq\hbar}\sqrt{1 - \left(\frac{2\mu + i\xi_n\hbar}{vq}\right)^2}\right.,\end{aligned} \tag{20}$$

where $g = 4$, $v \approx 10^6 \frac{\mathrm{m}}{\mathrm{s}}$ is the Fermi velocity in graphene layer and μ is the chemical potential which is equal to Fermi energy $\varepsilon_F = \hbar v k_F$ with $k_F = \sqrt{\frac{4\pi\rho}{g}}$ and ρ is the average electron density. In the case of undoped graphene layers the previous form simplifies substantially. The final dielectric response function is then expressed as

$$\varepsilon(q, i\xi_n) = 1 + \frac{\pi\alpha g c q}{8\varepsilon_m\sqrt{(vq)^2 + \xi_n^2}}, \tag{21}$$

where $\alpha = \frac{e^2}{4\pi\varepsilon_0\hbar c} \approx \frac{1}{137}$ is the electromagnetic fine-structure constant.

6 Casimir – vdW effects in graphene systems[2]

All calculations were done at a temperature of 300 K and at a fixed thickness of graphene layer 0.1 nm. The following results were made for a bilayer ***graphene – graphene system***, a ***graphene – substrate system*** with SiO_2 as a substrate and a ***multilayer system*** of graphene layers. Calculations have been done for doped and undoped graphene layers in all mentioned cases. At the end of the chapter, a table of all magnitudes for different distances is given for orientation in **Tab. 2**.

6.1 Bilayer graphene system (GGS)

The bilayer system is presented in **Fig. 3**. *L* and *R* are left and right semi-infinite vacuum spaces, *B* is the interlayer vacuum space, and *A* are the graphene layers.

In this case, the free energy takes a form of

$$\frac{\mathcal{F}_{gg}(b)}{S} = k_B T \sum_{q} \sum_{n=0}^{\infty} \ln\left[1+\frac{D_1(i\xi_n)}{D_2(i\xi_n)} e^{-2b\kappa_B(i\xi_n)}\right], \tag{22}$$

where ξ_n are the Matsubara frequencies, ε_i is the dielectric permittivity of a layer and D_1, D_2 are the previously mentioned secular determinants one for each layer.

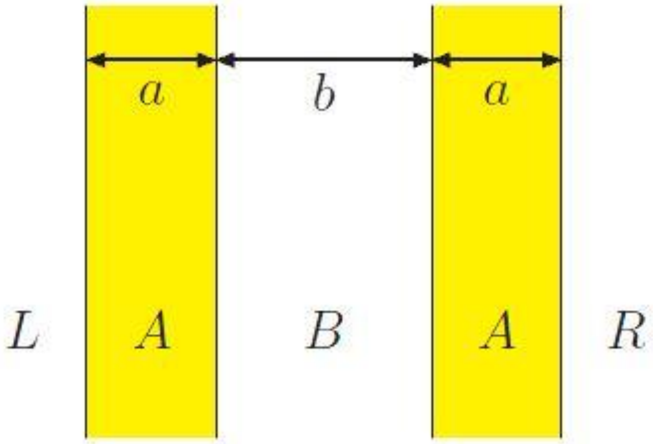

Figure 3 - A schematic presentation of a GGS system – two graphene sheets of finite thickness at a separation of *b*. The thickness of the left and right layer is *a*. We have labeled the left semi-infinite vacuum layer with *L*, the graphene layers with *A*, the intervening vacuum layer with *B* and the right vacuum layer with *R*

---

[2] This chapter is a rough remake of an article in the reference [6]

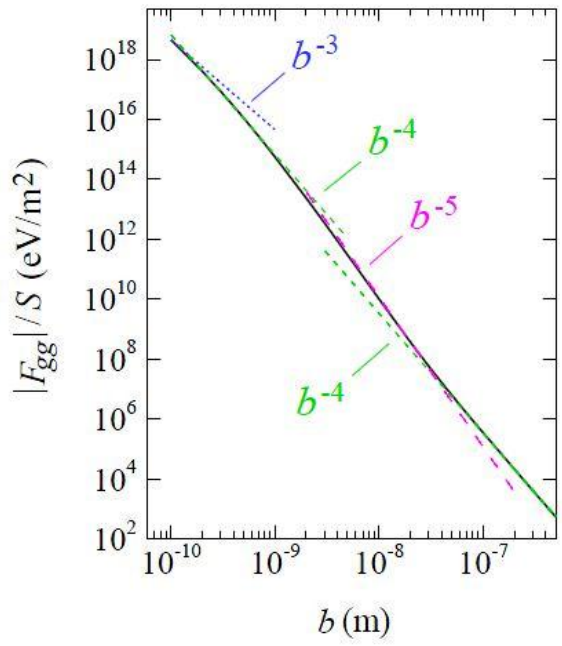

Figure 4 - Magnitude of the free energy per unit area of the GGS system for two undoped layers at T=300 K. The function is compared to the plotted scaling exponents as a function of separation *b*.

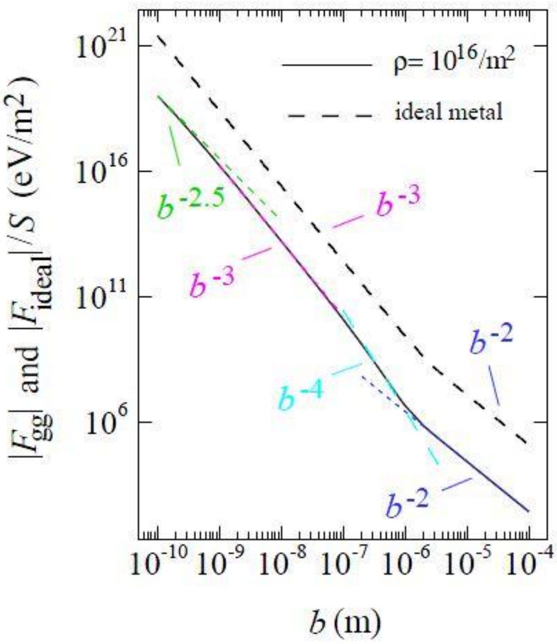

Figure 5 - Magnitude of the free energy per unit area of the GGS system for two doped layers (solid line) and ideal metal (dashed line) at T=300 K. The function is compared to the plotted scaling exponents as a function of separation *b*.

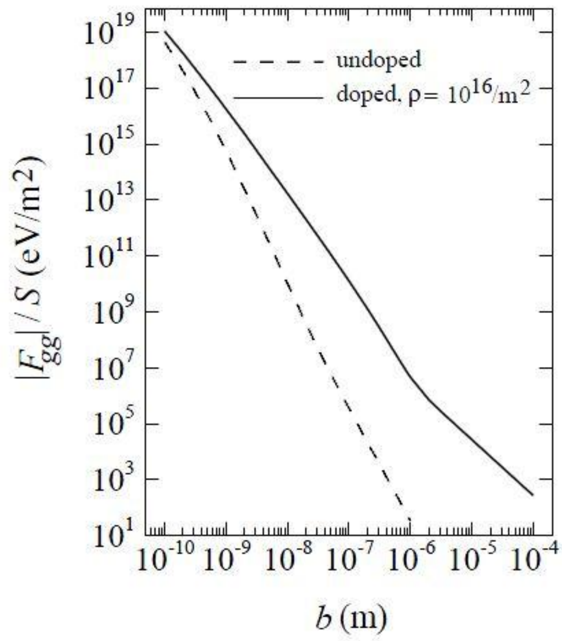

Figure 6 – Comparison of the magnitude of the free energy per unit area of the GGS system for the case of two doped (solid line) and undoped (dashed line) graphene layers. The magnitude of the free energy is higher for the case of doped graphene layers.

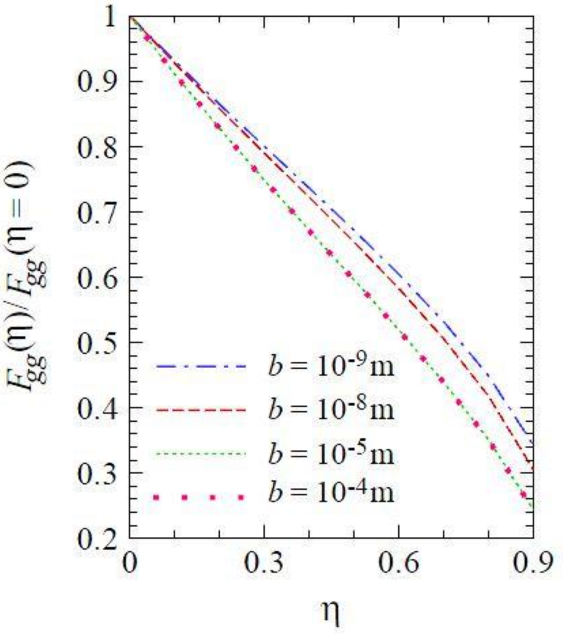

Figure 7 – The rescaled magnitude of free energy for the GGS system composed of two asymmetrically doped graphene layers as a function of the parameter of asymmetry. The plot is done for different interlayer separations of b = 1 nm, 10 nm, 10 µm, 100 µm. Note that the asymmetry effects are largest at small separations. $\mathcal{F}_{gg}(\eta = 0)$ has been calculated for the case of two identically doped layers at $\rho = 10^{16}\,\mathrm{m}^{-2}$.

Calculations and evaluation:

In **Fig. 4** one can observe the expected transitions for undoped graphene that go from vanishing distances to the non-retarded regime with *n=4*, then entering the retarded regime with *n=5* and finally the long distance limit with *n=4*.

Fig. 5 presents the plot for the doped graphene and includes results for an ideal metal. It is obvious that the magnitude of the free energy at a fixed distance is higher with better conductivity, so here we see the motivation for doping graphene layers. The direct effects of doping the graphene layer are seen in comparison with the undoped layer in **Fig.6**. The transitions here are not as obvious as before. When leaving vanishing distances, we enter a relatively broad regime with *n=3,4*, and then enter the long distance regime with *n=2*. In this case only these two regimes are recognizable.

One may stop here and remember the Casimir energy we derived earlier for the case of ideal metals and see that the scaling factor there is not the same as for the case of two ideal metals in this case. It should be noted, that previous calculations were done at a zero temperature limit and in this case they were not.

Another interesting case is what happens with the free energy when the graphene plates are asymmetrically doped. Let us introduce the dimensionless parameter of asymmetry $\eta = \frac{\rho_1 - \rho_2}{\rho_1 + \rho_2}$, where ρ_1 and ρ_2 are the electron densities in the plates.

The former is fixed at $\rho_1 = 10^{16}\,\frac{1}{\mathrm{m}^2}$ and the other is varied. When $\eta = 0$ there is no asymmetry between the layers, leading to no change, because both layers are doped with $\rho_1 = \rho_2 = 10^{16}\,\frac{1}{\mathrm{m}^2}$. If $\eta = 1$ then one of the plates is not doped at all, while the other still has the same electron density as before. **Fig. 7** presents the plot of the rescaled free energy $\frac{\mathcal{F}_{gg}(\eta)}{\mathcal{F}_{gg}(\eta = 0)}$ for the system of two graphene layers as a function of asymmetry for different values of the distance *b*. Note that at large separations the curves tend to coincide and become indistinguishable, making the asymmetry effects largest at small separations of the layers.

6.2 Graphene – Substrate system (GSS)

The GSS system is presented in **Fig. 8**. A single layer is not stable on its own, but stable in a multilayer system or apposed on a substrate. *L* and *R* are left and right semi-infinite spaces, *L* is a substrate (usually SiO_2) and *R* is a layer of vacuum, *B* is the interlayer vacuum space, and *A* is the graphene layer. In this case, the free energy takes a form of

$$\frac{\mathcal{F}_{gs}(b)}{S} = k_B T \cdot \sum_{q} \sum_{n=0}^{\infty} \ln\left[1 + \frac{\Delta_{AB} + \Delta_{RA} e^{-2a\kappa_a}}{1 + \Delta_{AB}\Delta_{RA} e^{-2a\kappa_a}} \Delta_{BL} e^{-2b\kappa_b}\right] \qquad (23)$$

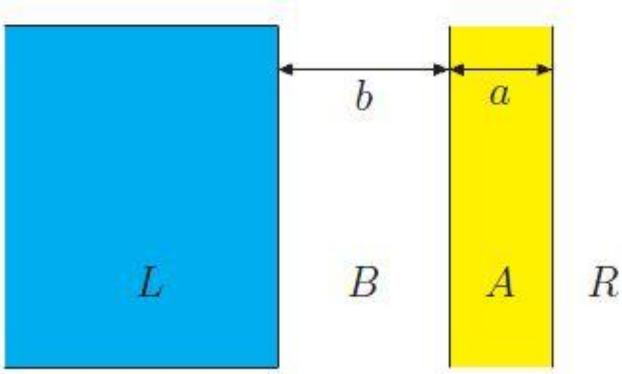

Figure 8 - A schematic presentation of a GSS system – a graphene layer of finite thickness at a separation of *b* from the apposed substrate. The thickness of the graphene layer is *a*. We have labeled the left semi-infinite substrate layer with *L*, the graphene layers with *A*, the intervening vacuum layer with *B* and the right vacuum layer with *R*.

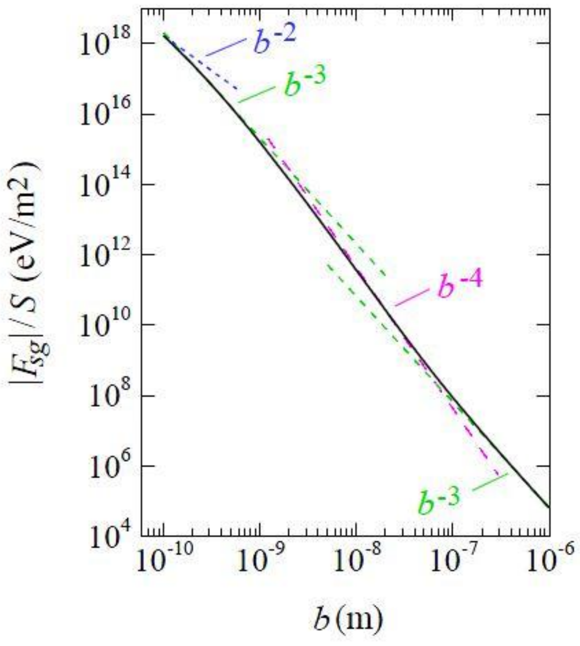

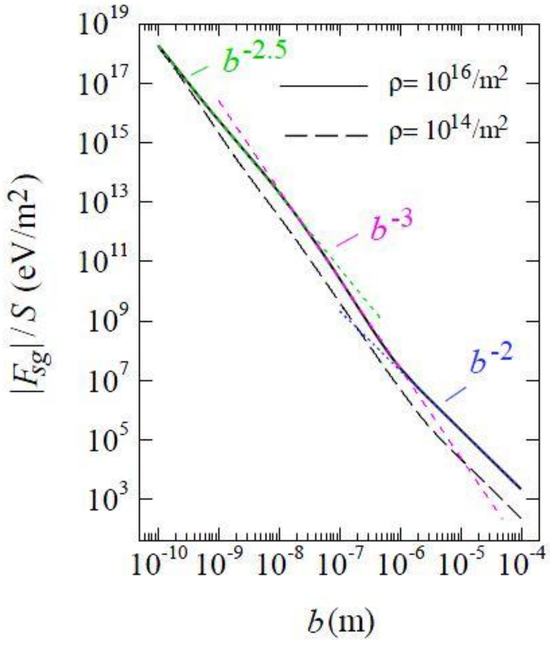

Figure 9 - Magnitude of the free energy per unit area of the GSS system for undoped graphene at T=300 K. The function is compared to the plotted scaling exponents as a function of separation *b*.

Figure 10 - Magnitude of the free energy per unit area of the GSS system for doped graphene at T=300 K for two different charge carrier densities. The function is compared to the plotted scaling exponents as a function of separation *b*.

Calculations and evaluation:

Results in **Fig. 9** are very similar to the ones before. Again the expected transitions can be seen for undoped graphene that go from vanishing distances to the non-retarded regime with *n=3*, entering the retarded regime with *n=4* and again the long distance limit with *n=5*, as predicted in **Tab. 1**.

In the case of doped graphene in **Fig. 10** the conclusions are also very similar to the ones in GGS system. The plot is done for two different electron densities of the graphene layer. Beyond vanishing distances, we enter the broad regime with a scaling exponent *n=3*, and then the long distance regime with *n=2*. These are the only two recognizable regimes.

6.3 Multilayer graphene system (MGS)

The MGS system is presented in **Fig. 11**. *L* and *R* are left and right semi-infinite substrates that will be assumed to be layers of vacuum. There are *N* layers of *B* as the interlayer vacuum space, and *N+1* layers of *A* as the graphene layer. For very large values of *N*, the free energy behaves as a linear function of the number of layers and takes a form of

$$\mathcal{F}_N(a,b) = N \cdot f_{gg}(a,b), \tag{24}$$

where the effective pair interaction between two neighboring layers is

$$f_{gg}(a,b) = k_B T \cdot \sum_q \sum_{n=0}^{\infty} \ln\left[\frac{1-\Delta^2(e^{-2\kappa_A a}+e^{-2\kappa_B b})+e^{-2(\kappa_A a+\kappa_B b)}}{2(1-\Delta^2 e^{-2\kappa_A a})} + \sqrt{\frac{G(a,b,\Delta)}{(1-\Delta^2 e^{-2\kappa_A a})^2}}\right]. \tag{25}$$

Other undefined quantities in the equation are

$$\begin{aligned} G(a,b,\Delta) &= (1-e^{-2(\kappa_A a+\kappa_B b)})^2 \\ &-2\Delta^2[(e^{-2\kappa_A a}+e^{-2\kappa_B b})(1+e^{-2(\kappa_A a+\kappa_B b)}) \quad \text{and} \quad \Delta = \frac{\kappa_A\varepsilon_B-\kappa_B\varepsilon_A}{\kappa_A\varepsilon_B+\kappa_B\varepsilon_A}, \\ &-4e^{-2(\kappa_A a+\kappa_B b)}]+\Delta^4(e^{-2\kappa_A a}+e^{-2\kappa_B b})^2 \end{aligned} \tag{26}$$

which again are all quantities that are derived from the boundary conditions and material properties.

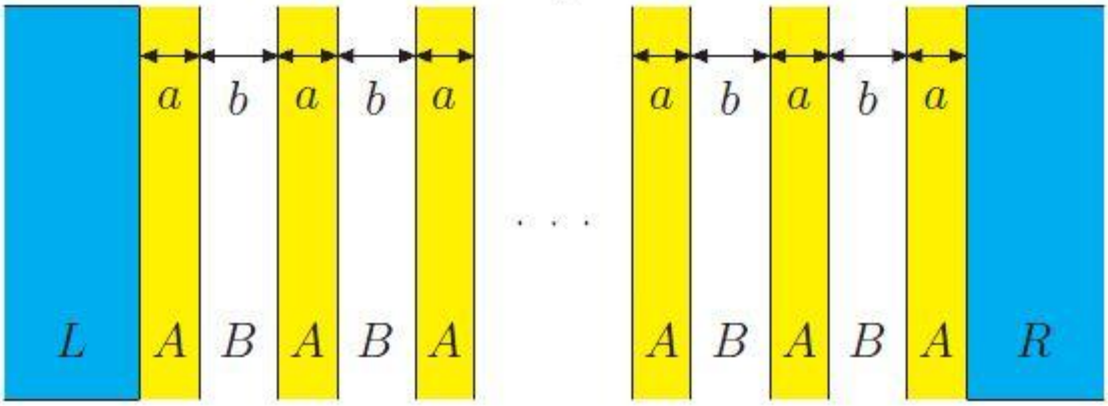

Figure 11 - A schematic presentation of a MGS system – *N+1* layers of graphene at separation of *b and* thickness of *a*, and *N* intervening layers of vacuum. We have labeled the left semi-infinite substrate layer with *L*, the graphene layers with *A*, intervening vacuum layers with *B* and the right substrate layer with *R*. *L* and *R* will be assumed to be layers of vacuum.

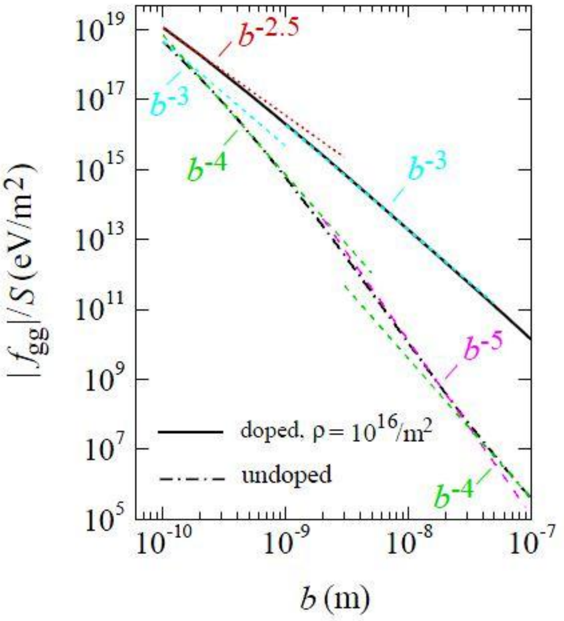

Figure 12 - Magnitude of the free energy per unit area and per number of layers of the MGS system at 300 K for *N+1* doped (solid line) and undoped (dot-dashed line) layers of graphene. The function is compared to the plotted scaling exponents as a function of separation *b*.

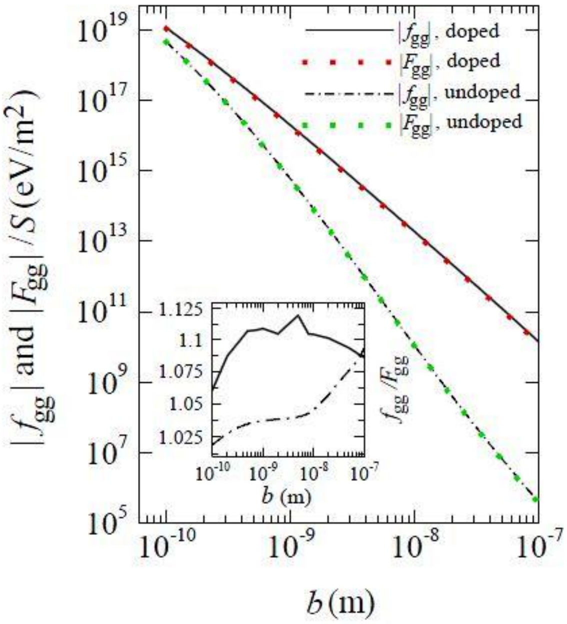

Figure 13 - Magnitude of the free energy per unit area and per number of layers of the MGS system at 300 K for *N+1* doped (solid line) and undoped (dot-dashed line) layers of graphene compared to the magnitude of the free energy per unit area for the GGS system composed of only two doped (red dotted line) and undoped (green dotted line) layers of graphene. The insert shows the ratio of these quantities for the doped (solid line) and undoped (dot-dashed line) case.

Calculations and evaluation:

Fig. 12 presents a plot of effective pair interaction free energy per unit area per number of layers calculated for doped and undoped graphene. One can see in **Fig. 13** that these calculations almost coincide with free energy per unit area of the bilayer graphene system. The results are almost the same, which means all transitions in **Fig. 12** are same as mentioned before for the bilayer graphene system.

Another plot is given inside of **Fig. 13** which presents the ratio between effective pair interaction free energy and bilayer graphene free energy for the doped and undoped version. The ratio is not equal to 1 but varies with distance and is never weaker compared to the one from GGS system. All we can say here is that differences occur due to many-body effect, because of the many constituents in our system.

6.4 Table of magnitudes ($\rho_1 = 10^{16}\frac{1}{\mathrm{m}^2}$, $\rho_2 = 10^{14}\frac{1}{\mathrm{m}^2}$)

b\FE	GGS: ρ=0	GGS: ρ₁	GSS: ρ=0	GSS: ρ₁	GSS: ρ₂	MGS: ρ=0	MGS: ρ₁
1 nm	564 eV	17.7 keV	1.57 keV	5.77 keV	2.12 keV	590 eV	19.6 keV
10 nm	0.01 eV	16.9 eV	0.36 eV	21.1 eV	3.28 eV	0.01 eV	18.7 eV
100 nm	3.6E-7 eV	0.01 eV	8.7E-5 eV	0.027 eV	4.2E-3 eV	3.9E-7 eV	0.014 eV

Table 2 - List of free energy magnitudes for 3 different distances and for different types of body systems

7 Conclusion

We presented the Casimir force in perfect metals and the Casimir – vdW effects in real materials. We have seen that these forces can be large at the right distances, which gives the direct impact in technology. Specifically we have studied the interactions between two and *N+1* graphene sheets and between a graphene sheet and a SiO_2 substrate. The calculations were done in the frame of Lifshitz theory and the results were presented in the form of the magnitude of free energy per unit area, which is a quantity that is directly connected to the Casimir – vdW effects between given objects. All these cases that have been analyzed and discussed above are relevant for many realistic geometric and nanoscopic scale systems. The main motivation for a detailed study of Casimir – vdW interactions between graphene sheets in graphite like geometries is the fact that graphitic systems belong to closed shell systems and thus display no covalent bonding, so any bonding interaction is by necessity of a Casimir – vdW type.

8 References

[1] *Focus: The Force of Empty Space*, Phys. Rev. Focus **2**, 28 (1998)

[2] V. A. Parsegian, P. L. Hansen, R. Podgornik, J. Chem. Phys., **119**, No. 2, 8 (2003)

[3] J. Mahanty and B. W. Ninham, *Dispersion Forces*, (Academic, London, 1976)

[4] S. K. Lamoreaux, Phys. Rev. Lett. **78**, 5–8 (1997)

[5] R. Podgornik and A. Vilfan, *Elektromagnetno polje* (script, v. 20.9.2011, pg. 187)

[6] J. Sarabadani, A. Naji, R. Asgari, R. Podgornik, arXiv:1105.4241v1 (2011)

[7] A. K. Geim and K. S. Novoselov, Nature Materials **6**,183–191 (2007)

[8] R. Heyrovska, arXiv:0804.4086 (2008)

[9] *Van der Waals Retardation Effects*, (University of Washington, Handout)

[10] C. Zhihong and V. Perebeinos, Nature Nanotechnology **2**, 605 - 615 (2007)

[11] E.H. Hwang and S. D. Sarma, Phys. Rev. **B 75**, 205418 (2007)

[12] V. A. Parsegian, *Van der Waals Forces: A Handbook for Biologists, Chemists, Engineers, and Physicists*, (Cambridge University Press, New York, 2006)